

SimuQ: A Domain-Specific Language For Quantum Simulation With Analog Compilation

YUXIANG PENG, University of Maryland, United States

JACOB YOUNG, University of Maryland, United States

PENGYU LIU, Tsinghua University, China

XIAODI WU, University of Maryland, United States

Hamiltonian simulation is one of the most promising applications of quantum computing. Recent experimental results suggest that continuous-time analog quantum simulation would be advantageous over gate-based digital quantum simulation in the Noisy Intermediate-Size Quantum (NISQ) machine era. However, programming such analog quantum simulators is much more challenging due to the lack of a unified interface between hardware and software, and the only few known examples are all hardware-specific. In this paper, we design and implement SimuQ, the first domain-specific language for Hamiltonian simulation that supports pulse-level compilation to heterogeneous analog quantum simulators. Specifically, in SimuQ, front-end users will specify the target Hamiltonian evolution with a Hamiltonian modeling language, and the programmability of analog simulators is specified through a new abstraction called the abstract analog instruction set by hardware providers. Through a solver-based compilation, SimuQ will generate the pulse-level instruction schedule on the target analog simulator for the desired Hamiltonian evolution, which has been demonstrated on pulse-controlled superconducting (Qiskit Pulse) and neutral-atom (QuEra Bloqade) quantum systems, as well as on normal circuit-based digital quantum machines. Moreover, we also demonstrate the advantage of analog compilation over digital compilation on IBM machines, the use of SimuQ for resource estimation for hypothetical machines, and a scalability test of SimuQ's compilation.

Additional Key Words and Phrases: quantum simulation, analog quantum computing, pulse-level programming

1 INTRODUCTION

Motivation. The development of appropriate abstraction is a critical step in the design of programming languages, which will help bridge the domain users and the potentially complicated computing devices, and is hence a fundamental factor of the productivity of the underlying programming language. Prominent early examples of such include, e.g., FORTRAN [Backus 1978] and SIMULA [Nygaard and Dahl 1978], both of which provide high-level abstractions for modeling desirable operations for domain applications and have been proven a huge success in history.

Conventionally, (qubit-level) quantum circuits have been adopted as the major abstraction for quantum computing, which is mathematically simple and works well as a mental tool for the theoretical study of quantum information. Because of that, many quantum programming languages [Abhari et al. 2012; Green et al. 2013; Hietala et al. 2021; Liu et al. 2019] have adopted quantum circuits as the only abstraction.

While successful when working with quantum applications involving a handful of qubits, quantum circuit abstraction is conceivably hard to scale even when we have e.g., hundreds of qubits,

Our code is available at <https://github.com/PicksPeng/SimuQ>.

A project website of SimuQ is available at <https://pickspeng.github.io/SimuQ/>.

Authors' addresses: Yuxiang Peng, Department of Computer Science and Joint Center for Quantum Information and Computer Science, University of Maryland, United States, ypeng15@umd.edu; Jacob Young, Department of Electrical & Computer Engineering and Joint Center for Quantum Information and Computer Science, University of Maryland, United States, jyoung25@umd.edu; Pengyu Liu, Institute for Interdisciplinary Information Sciences, Tsinghua University, China, liupengy19@mails.tsinghua.edu.cn; Xiaodi Wu, Department of Computer Science and Joint Center for Quantum Information and Computer Science, University of Maryland, United States, xwu@cs.umd.edu.

which already makes visualizing quantum circuits a hard task. Moreover, it also requires the specification of (qu)bit-level quantum operations, which needs strong quantum expertise, could change significantly for different hardware, and stays at a too-detailed level for domain experts.

Quantum Hamiltonian simulation is arguably one of the most promising quantum applications, the programming of which, however, has been quite a non-trivial task. In a seminal project [Childs et al. 2018], the authors have spent nearly two years in programming a few major quantum simulation algorithms for the 1-D Heisenberg model in Quipper [Green et al. 2013] due to many sophisticated implementation details at the circuit level. Developing a better abstraction for quantum Hamiltonian simulation is highly desirable for the productivity of these domain applications.

We propose to separate the description of the target Hamiltonian simulation, which is a physics object, from its implementation on specific quantum hardware, which consists of a schedule of instructions available on quantum devices. As a result, the domain experts can focus on describing the desired Hamiltonian simulation through a newly developed modeling programming language and leave its implementation—a tedious and error-prone procedure—to be handled by the compiler.

An exciting new opportunity exposed by this new abstraction is the compilation to general quantum devices that are not gate-based. Indeed, recent experimental developments [Ebadi et al. 2021; Semeghini et al. 2021] suggest that continuous-time analog quantum simulators could be advantageous over gate-based digital quantum simulation in the NISQ [Preskill 2018] era. Operations on these analog quantum simulators are pieces of specific Hamiltonian evolution on a small fraction of the system which are controlled directly by continuous-time pulses rather than gates. In fact, all digital quantum gates are eventually implemented by pulses in a similar way. However, by breaking the gate abstraction and allowing a direct compilation to pulses, a lot of resources could be saved [Shi et al. 2020], which is critical for the performance of NISQ devices. We are inspired to develop a compilation procedure to leverage this benefit for Hamiltonian simulation, which would also work with analog quantum simulators that are based on different physical implementation.

Hamiltonian Simulation. Mathematically, Hamiltonian simulation refers to evolving a quantum state $|\psi(t)\rangle$, which is a high-dimensional complex vector, according to the *Schrödinger* equation:

$$\frac{d}{dt} |\psi(t)\rangle = -iH(t) |\psi(t)\rangle, \quad (1.0.1)$$

where $H(t)$ is generally a time-dependent Hermitian matrix, also known as the Hamiltonian governing the system. For an n qubit system, the dimension of both $H(t)$ and $|\psi(t)\rangle$ could be 2^n , which makes its classical simulation exponentially difficult. However, by carefully scheduling available instructions on a quantum device, one could let the quantum device simulate the target Hamiltonian $H(t)$ with the device’s own Hamiltonian evolution, incurring minimal overhead.

Technical Challenges. There are a few design choices and technical challenges toward the development of the new abstraction, associated domain-specific language, and its compilation,

The *first* one is the precise modeling of Hamiltonian simulation and potentially heterogeneous analog devices. The former is intuitive as our object of interest is $H(t)$, whereas its exponential-size matrix expression is less desirable due to the scalability. Inspired by popular computational physics packages (e.g., QuTiP [Johansson et al. 2012]), we symbolically describe $H(t)$ as the sum of Hamiltonians that are tensor products of local ones, which leads to a very succinct description that is yet rich enough to express most interesting quantum many-body systems for simulation.

The modeling of analog quantum devices is much more challenging. Unlike the gate model where the fundamental primitives are a finite number of one or two-qubit unitaries, analog quantum devices are usually described by one global Hamiltonian, which differs significantly device by device [QuEra 2022; Semeghini et al. 2021; Silvério et al. 2022]. Inspired by the underlying control of these Hamiltonians, we propose a new abstraction called the *Abstract Analog Instruction Set* (AAIS)

to describe the programmability of heterogeneous analog devices. Precisely, we use *signal lines* to model carriers of analog signals, each of which could carry different patterns of analog pulses that are abstracted as parameterized *analog instructions*. These parameterized analog instructions would then implement pieces of Hamiltonian simulations on some fraction of the system, the collection of which is a representation of the programmability of the analog device.

The *second* challenge is the compilation to analog quantum devices. In the digital setting, the primitive gates are small-dimensional matrices, and the compilation of large quantum evolution into these gates could be done with analytical formula (e.g., the Solovay-Kitaev theorem [Kitaev 1997]). In the analog setting, the effect of performing an instruction ι with parameter valuation v is described as a time-independent Hamiltonian $H_{(\iota, v)}$. An analog instruction schedule \mathcal{S} assigns signal line L to one instruction ι with a valuation v (denoted as $\mathcal{S}(L, t) = (\iota, v)$) at any time t , whose total effect is the summation of effects from all signal lines, i.e., $H^{\mathcal{S}}(t) = \sum_L H_{\mathcal{S}(L, t)}$. The goal of the compilation is to match $H^{\mathcal{S}}(t)$ with $H(t)$, which we have handled as symbolic pattern matching inspired by the seminal work in classical analog compilation [Achour et al. 2016]. This restriction improves the scalability of the compilation, which, however, unfortunately ignores possible instruction schedules whose validity relies on the matrix semantics of $H^{\mathcal{S}}(t)$ and $H(t)$.

Given a valid instruction schedule \mathcal{S} , the last challenge is to convert \mathcal{S} into the actual pulses executable on target devices, which is not readily supported by any existing quantum programming tool-chain, and we have to engineer the desired pulse shapes ourselves for several devices.

Contributions. Based on our new abstraction, we design and implement a domain-specific Simulation language for Quantum (SimuQ) in Python, as well as its compiler for heterogeneous analog devices specified by AAIS. We start with a running example in Sect. 2. A precise formulation of the Hamiltonian modeling language and the abstract analog instruction set are given in Sect. 3. We describe the construction of SimuQ’s compiler and its error analysis in Sect. 4. An extensive use case study (e.g., compilation to multiple platforms, comparison with digital compilation, and resource estimation of hypothetical machines) and a scalability test of SimuQ are included in Sect. 5.

Related Works. To our best knowledge, SimuQ is the first domain-specific programming language for quantum simulation that supports pulse-level compilation to analog quantum devices. Computational quantum physics packages like QuTiP [Johansson et al. 2012] map descriptions of Hamiltonians into their matrix representations for classical simulation, without any compilation to quantum devices. There are a few pulse-level programming interfaces for quantum devices such as IBM Qiskit Pulse [Cross et al. 2022], QuEra Bloqade [QuEra 2022], and Pasqal Pulser [Silvério et al. 2022]. However, these interfaces are designed to represent the specific underlying quantum hardware rather than to provide a unified interface for all analog quantum devices like AAIS. Moreover, no compilation from Hamiltonian description is pursued in these tools. Finally, SimuQ’s solver-based compilation is inspired by the seminal work in classical analog compilation [Achour and Rinard 2020; Achour et al. 2016], although the specific abstraction and compilation technique therein is less relevant as the nature of analog quantum devices is very different from classical ones.

2 RUNNING EXAMPLE

We present an example as a concrete illustration of our framework. We introduce: (1) a Hamiltonian simulation problem encoded in the Hamiltonian modeling language; (2) an AAIS describing a Rydberg atom quantum system; (3) the resulting pulses for machine execution.

2.1 Quantum Preliminaries

A *qubit* (or *quantum bit*) is the analogue of a classical bit in quantum computation. It is a two-level quantum-mechanical system described by the Hilbert space \mathbb{C}^2 . The classical bits “0” and “1” are

represented by the qubit states $|0\rangle = \begin{bmatrix} 1 \\ 0 \end{bmatrix}$ and $|1\rangle = \begin{bmatrix} 0 \\ 1 \end{bmatrix}$, and linear combinations of $|0\rangle$ and $|1\rangle$ are also valid states, forming a *superposition* of quantum states. An n -qubit state is a unit vector in the Kronecker tensor product \otimes of n single-qubit Hilbert spaces, i.e., $\mathcal{H} = \otimes_{i=1}^n \mathbb{C}^2 \cong \mathbb{C}^{2^n}$, whose dimension is exponential in n . For an n by m matrix A and a p by q matrix B , their Kronecker product is an np by mq matrix where $(A \otimes B)_{pr+u,qs+v} = A_{r,s}B_{u,v}$. The *complex conjugate transpose* of $|\psi\rangle$ is denoted as $\langle\psi| = |\psi\rangle^\dagger$ (\dagger is the Hermitian conjugate). Therefore, the *inner product* of ϕ and ψ could be written as $\langle\phi|\psi\rangle$.

The time evolution of quantum states is specified by a time-dependent Hermitian matrix $H(t)$ over the corresponding Hilbert space, known as the *Hamiltonian* of the quantum system. Typical single-qubit Hamiltonians include the famous *Pauli matrices*:

$$I = \begin{bmatrix} 1 & 0 \\ 0 & 1 \end{bmatrix}, \quad X = \begin{bmatrix} 0 & 1 \\ 1 & 0 \end{bmatrix}, \quad Y = \begin{bmatrix} 0 & -i \\ i & 0 \end{bmatrix}, \quad Z = \begin{bmatrix} 1 & 0 \\ 0 & -1 \end{bmatrix}. \quad (2.1.1)$$

Specifically, we write the number operator $\hat{n} = (I - Z)/2$, which determines if the state is in $|1\rangle$. A multi-qubit Hamiltonian can be a linear combination of product Hamiltonians — tensor products of Pauli matrices. By convention, we write X_j for a multi-qubit Hamiltonian to indicate $I \otimes \dots \otimes I \otimes X \otimes I \otimes \dots \otimes I$, where the j -th operand is X . Similarly we write Y_j and Z_j . These notations represent operations on the j -th subsystem. The time evolution obeys the *Schrödinger equation* (1.0.1).

Physically, operators in Hamiltonians correspond to physics effects like the influence of electrical or magnetic fields. Scalar multiplication (e.g., $2 \cdot X$) changes the effect strength: if strength doubles, the time to achieve the same evolution is halved. Additions of operators (e.g., $X_1 + X_2$) represent simultaneous physics effects, e.g., the superposition of forces. Multiplications of operators (e.g., $X_1 X_2$) represent the interactions across different sites.

Quantum measurement refers to the process to extract classical information from quantum systems. When applied to state $|\phi\rangle$, with probability $|\langle s|\phi\rangle|^2$, it reports the bit-string s and collapses the quantum state $|\phi\rangle$ to a classical state $|s\rangle = |s_1\rangle \otimes |s_2\rangle \otimes \dots \otimes |s_n\rangle$.

2.2 Compiling a Hamiltonian to Rydberg Systems

Quantum simulation is to reproduce the evolution of a target quantum system on another programmable quantum system (backend). Suppose the target system evolves under Hamiltonian $H(t)$ over Hilbert space \mathcal{H}_1 and we want to simulate it on the backend whose Hilbert space is \mathcal{H}_2 . We need to find a subspace $\mathcal{H}'_2 \subset \mathcal{H}_2$ satisfying $\mathcal{H}_1 \cong \mathcal{H}'_2$, a linear mapping $\mathcal{A} : \mathcal{H}_1 \rightarrow \mathcal{H}'_2$, and a programmed evolution on the backend where the evolution limited in \mathcal{H}'_2 is governed by $\mathcal{A}(H(t))$.

Consider a toy example where the user wants to simulate a three-qubit system evolving under a time-independent Hamiltonian

$$H_{\text{tar}}(t) = -(\hat{n}_1 + \hat{n}_2 + \hat{n}_3) + 2(X_1 + X_2 + X_3) + 4(\hat{n}_1 \hat{n}_2 + \hat{n}_2 \hat{n}_3) \quad (2.2.1)$$

for time duration $t \in [0, 1]$. The physical meaning of this Hamiltonian will be discussed further in Section 5.1.

The user would like to compile this system to an ideal three-qubit Rydberg atom array as the backend. Configurable Rydberg atoms arrays [Cong et al. 2022; Ebadi et al. 2022, 2021; Saffman 2016] are one of the most promising quantum platforms towards computational advantages, where neutral atoms are placed on a plane and interfered with by laser beams. On our backend, the positions of atoms can be arbitrarily configured. Between a pair of atoms, there are van der Waals forces [Beguin et al. 2013] attracting them. Written in quantum mechanics, the force between the

atom i and j is a Hamiltonian term

$$H_{\text{sys}}^{(i,j)}(t) = \frac{C}{d^6(i,j)} \hat{n}_i \hat{n}_j, \quad (2.2.2)$$

where the Rydberg interaction constant $C \approx 5.42 \times 10^6 \text{ MHz} \cdot \mu\text{m}^6$ and $d(i,j)$ is the distance between the two atoms. To interfere with the system, our backend has three laser beams, each targeting one of the atoms. The laser beam i is configured by three functions $\tilde{\Delta}_i(t)$, $\tilde{\Omega}_i(t)$ and $\tilde{\phi}_i(t)$, representing the detuning, the amplitude and the phase of the laser [Saffman 2016]. It interacts with the i -th atom according to a Hamiltonian term

$$H_{\text{las}}^{(i)}(t) = -\tilde{\Delta}_i(t) \hat{n}_i + \frac{\tilde{\Omega}_i(t)}{2} (\cos(\tilde{\phi}_i(t)) X_i - \sin(\tilde{\phi}_i(t)) Y_i). \quad (2.2.3)$$

Overall, if we configure the backend using atom positions $\{\vec{x}_i\}$ and laser $\{(\tilde{\Delta}_i(t), \tilde{\Omega}_i(t), \tilde{\phi}_i(t))\}$, the system evolves under Hamiltonian

$$H_{\text{backend}}(t) = H_{\text{las}}^{(1)}(t) + H_{\text{las}}^{(2)}(t) + H_{\text{las}}^{(3)}(t) + H_{\text{sys}}^{(1,2)}(t) + H_{\text{sys}}^{(2,3)}(t) + H_{\text{sys}}^{(1,3)}(t). \quad (2.2.4)$$

To simulate H_{tar} using the ideal Rydberg atom backend, we can manually generate a configuration easily. However, when the system size grows or machine effects become complicated for different architectures, manual generation tends to be impossible. We aim at a framework to automate the compilation of quantum simulation. In the following, we introduce how SimuQ tackles this problem.

2.2.1 Programming Quantum System in HML. We program $H_{\text{tar}}(t)$ in our Python implementation of the Hamiltonian Modeling Language (HML), as in Figure 1a. The program starts by specifying a quantum system QS and $N = 3$ qubit sites stored in q (lines 1-3). Passing QS into their initialization denotes them as sites of QS . Each qubit site contains fields representing the operators I , X , Y , and Z , and we create \hat{n}_i for each i with the expression $(q[i].I - q[i].Z) / 2$ (lines 4-5).

Next, we compose $H_{\text{tar}}(t)$ with these operators. We begin with an empty Hamiltonian h , program each term in H_{tar} , and add them into h (lines 6-11). In SimuQ's implementation, Hamiltonians are stored in a dictionary as linear combinations of product Hamiltonians. For example, the operator

```

1 QS = QSystem()
2 q = [qubit(QS)
3     for i in range(N)]
4 n = [(q[i].I - q[i].Z) / 2
5     for i in range(N)]
6 h = 0
7 for i in range(N) :
8     h += - n[i] + 2 * q[i].X
9 for i in range(N - 1) :
10    h += 4 * n[i] * n[i + 1]
11 MIS.add_evo(h, T)

```

(a) Hamiltonian (2.2.1) programmed in HML. Here $N = 3$ is the number of sites. $T = 1$ is the evolution time.

```

1 Rydberg = QMachine()
2 q = [qubit(Rydberg) for i in range(N)]
3 n = [(q[i].I - q[i].Z) / 2 for i in range(N)]
4 x = [0] + [GlobalVar(Rydberg) for i in range(1, N)]
5 h = 0
6 for i in range(N) :
7     for j in range(i) :
8         h += (C / (x[i] - x[j])**6) * n[i] * n[j]
9 Rydberg.set_sys_ham(h)
10 for i in range(N) :
11     L = SignalLine(Rydberg)
12     i = Instruction(L, 'native')
13     Δ, Ω, φ = LocalVar(i), LocalVar(i), LocalVar(i)
14     X_Y = cos(φ) * q[i].X - sin(φ) * q[i].Y
15     i.set_ham(-Δ * n[i] + Ω / 2 * X_Y)

```

(b) An AAIS for the ideal Rydberg system. $N = 3$ is the number of sites. C is the Rydberg interaction constant.

Fig. 1. Examples of HML and AAIS specification language implemented in Python.

Physics	Signal carrier	Engineered signal	Signal effect	Device evolution
AAIS	Signal line	Instruction	Instruction Hamiltonian	Total Hamiltonian
Rydberg Systems	Laser beam	Parameter pulses	Laser-atom interaction	System evolution

Table 1. The design of concepts in AAIS. The first row includes the common physics concepts of quantum devices. The second row presents our abstraction of these physics concepts in AAIS. The last row illustrates the concepts with their concrete correspondences in Rydberg systems.

$\hat{n}_1\hat{n}_2 = (I - Z_1)/2 \cdot (I - Z_2)/2 = (Z_1Z_2 - Z_1 - Z_2 + I)/4$ is stored as

$$\left\{ Z_1Z_2 : \frac{1}{4}, \quad Z_1 : -\frac{1}{4}, \quad Z_2 : -\frac{1}{4}, \quad I : \frac{1}{4} \right\}. \quad (2.2.5)$$

Without ambiguity, we overload the dictionary representation to denote the coefficients of product Hamiltonian in a Hamiltonian, e.g., write $\hat{n}_1\hat{n}_2[Z_1Z_2] = 1/4$.

After programming $H_{\text{tar}}(t)$ in \mathbf{h} , we add the evolution under time-independent Hamiltonian $H_{\text{tar}}(t)$ for duration T to the quantum system \mathbf{QS} , where $T = 1$ microsecond (line 12).

2.2.2 Describing Analog Quantum Devices by Abstract Analog Instruction Set. Different architectures of programmable quantum devices have vastly different physics and specifications. To have an automated framework for all kinds of devices, we propose abstract analog instruction sets (AAIS) to capture the capabilities of analog quantum devices. The design ideas of AAIS are presented in Table 1.

We abstract the common concepts for quantum devices first. Normally, there are signal carriers attached to a quantum device. Signals in the form of pulses (time-dependent functions) are sent through the carriers and create effects on the device. The effects may be direct or effective. Direct effects depict in every detail how the system changes according to signals. However, the devices are often too complicated to describe and hardware developers design engineered pulses such that the pulses effectively generate simple effects. These signals are also configurable through parameters like amplitudes and phases over time. Besides, there may be inherent dynamics of the quantum devices induced by the physics of the architecture. Overall, the evolution of the device obeys the Hamiltonian determined by signals' effects and inherent dynamics.

In an AAIS, signal carriers are abstracted as *signal lines*. Each signal line may contain several *instructions* to represent the signals sent through the carrier, and each time the signal line carries no more than one instruction. Instructions have properties distinguishing their compatibility with other instructions decided by their effects. Instructions causing direct effects are *native*, and those causing effective effects are *derived*. Derived instructions should not be simultaneously applied with other instructions affecting shared sites, since there might be crosstalks induced by the detailed implementation implicit in AAIS. To further configure the instructions, we declare several local variables to each instruction that can be tuned for each invocation to generate a variety of effects. With a valuation of these variables, the effect of the instruction is described by an *instruction Hamiltonian*. When invoking many instructions at the same time, their instruction Hamiltonians are summed up to constitute the Hamiltonian governing the evolution of the device. For those global configurable parameters and inherent dynamics, we model them as global variables and system instructions, which are configured and fixed for the whole evolution.

We illustrate our ideas above using a Rydberg AAIS designed for the ideal Rydberg system backend. The positions of atoms (assumed to be 1-D) in our ideal backend are configurable in the pre-experiment stage and unchangeable after evolution starts. They are modeled as global variables x_i , and the internal van der Waals forces are modeled as a system instruction t_{sys} whose instruction

Hamiltonian is

$$H_{\text{sys}}(t) = \sum_{1 \leq i < j \leq 3} C/(x_i - x_j)^6 \hat{n}_i \hat{n}_j. \quad (2.2.6)$$

The laser beams have direct effects on the system based on the parameters. For each laser beam, we declare a signal line L_i and an instruction ι_i containing three local variables Δ_i , Ω_i , and ϕ_i . The instruction Hamiltonian is then

$$H_{\iota_i, v_i}(t) = -\Delta_i \hat{n}_i + \Omega_i/2 \cdot (\cos(\phi_i) X_i - \sin(\phi_i) Y_i). \quad (2.2.7)$$

where Δ_i , Ω_i and ϕ_i use their valuation from v_i .

2.2.3 Programming the Rydberg AAIS. We now show how to program the Rydberg AAIS in our AAIS Specification Language, as displayed in Figure 1b.

First, as in HML, we define the quantum machine under the variable Rydberg, and we declare qubit sites belonging to the system and store them in list q (lines 1-2). Similar to HML, we can define number operators for the qubit sites in algebraic expressions (line 3). Then we set the atom coordinates in the 1-D space of the ideal Rydberg machine as global variables stored in list x (unit: μm) and fix the coordinate of the first atom at 0 (line 4). We build the system instruction $H_{\text{sys}}(t)$ by constructing each $H_{\text{sys}}^{(i,j)}$ term, adding them to h and setting h as a system Hamiltonian (lines 5-9). We model the i -th laser beam by a signal line L_i and package the effect $H_{\iota_i, v_i}(t)$ into an instruction ι_i (lines 11-12). The local variables are declared belonging to ι_i , corresponding to the three parameters respectively, and stored in Δ , Ω , and ϕ (line 13). ι_i is a native instruction since its effect is direct. We describe its instruction Hamiltonian with its variables and site operators of the system (lines 14-15).

For an instruction schedule \mathcal{S} where $\mathcal{S}(L_i, t) = (\iota_i, v_i(t))$ contains the instruction of signal line L_i and valuation $v_i(t)$ for variables Δ_i , Ω_i , and ϕ_i , the overall effect when applying \mathcal{S} on the machine then is:

$$H_{\text{Rydberg}}^{\mathcal{S}}(t) = H_{\text{sys}}(t) + \sum_{i=1}^N H_{\mathcal{S}(L_i, t)}. \quad (2.2.8)$$

2.2.4 AAIS for Other Systems. We also exhibit our AAIS design for IBM’s superconducting systems and IonQ’s trapped ion systems to show the generality of AAIS to capture the capabilities of different quantum systems.

AAIS for Superconducting Transmon Systems. IBM’s superconducting quantum processors [Jurcevic et al. 2021; Steffen et al. 2011] construct transmon qubits from fixed-frequency anharmonic oscillators coupled to neighboring sites. Each transmon qubit is driven by microwaves inducing the single-qubit Hamiltonian $\alpha(\cos(\theta)X_i + \sin(\theta)Y_i)$ where α and θ are tunable parameters corresponding to the amplitude and phase of the microwave. We create signal line L_i corresponding to the driving microwave for the i -th qubit, containing a native instruction ι_i^{X-Y} with local variables α and θ . Z_i evolution is effectively achieved by tuning phases of future microwaves, hence it cannot be activated simultaneously with other instructions. We declare it as a derived instruction ι_i^Z belonging to L_i realizing αZ_i with variable α .

Two-qubit interactions are realized by echoing cross-resonance microwaves, effectively approximating evolution under $Z_i X_j$ for neighboring i, j in the machine topology. Together with single qubit evolution, this interaction can realize $X_i X_j$, $Y_i Y_j$, or $Z_i Z_j$. For any edge (i, j) in the machine topology graph E , we create a signal line L_{ij} with three derived instructions realizing $\alpha P_i P_j$ for $P \in \{X, Y, Z\}$ respectively.

	H_{sys}	H_{t_1}	H_{t_2}	\dots	H_{MIS}	
$Z_1 Z_2$	$\frac{C}{4(x_1 - x_2)^6}$	+	+	+	\dots	$= 1$
$Z_2 Z_3$	$\frac{C}{4(x_2 - x_3)^6}$	+	+	+	\dots	$= 1$
Z_1	$-\frac{C}{4(x_1 - x_2)^6} - \frac{C}{4(x_1 - x_3)^6}$	$+$	$\frac{1}{2} \Delta_{t_1} s_{t_1}$	+	\dots	$= -\frac{1}{2}$
Z_2	$-\frac{C}{4(x_1 - x_2)^6} - \frac{C}{4(x_2 - x_3)^6}$	+	+	$\frac{1}{2} \Delta_{t_2} s_{t_2}$	+	$= -\frac{3}{2}$
\vdots	\vdots	\vdots	\vdots	\vdots	\vdots	\vdots

→ $\begin{cases} x_1 \triangleq 0 \\ x_2 = 10.52 \\ x_3 = 21.04 \\ s_{t_1} = s_{t_2} = s_{t_3} = 1 \\ \Delta_{t_1} = \Delta_{t_3} = 1.03 \\ \Delta_{t_2} = 1 \\ \Omega_{t_1} = \Omega_{t_2} = \Omega_{t_3} = 4 \\ \phi_{t_1} = \phi_{t_2} = \phi_{t_3} = 0 \end{cases}$

Fig. 2. The equation system to synthesize H_{MIS} on the ideal Rydberg machine, and the solution to the equation system.

For an N -qubit machine with topology E , the total effect of a schedule S is

$$H_{\text{IBM}}^S(t) = \sum_{i=1}^N H_{S(L_i, t)} + \sum_{(i, j) \in E} H_{S(L_{ij}, t)} \quad (2.2.9)$$

AAIS for Trapped Ion Systems. IonQ’s trapped ion systems [Bruzewicz et al. 2019; Debnath et al. 2016; Grzesiak et al. 2020] create chains of Yb^+ ion potential traps and use lasers to affect the ions. Their machines have single qubit $(\cos(\theta)X_i + \sin(\theta)Y_i)$ evolution, Z_i rotations, and $X_i X_j$ evolution between arbitrary two qubits. Using them, $Y_i Y_j$ and $Z_i Z_j$ evolutions are realizable, resulting in a similar AAIS to IBM’s, where 2-qubit instructions are between every pair of qubits.

2.2.5 Compilation to Executable Pulses. We then walk through the compilation of H_{tar} to the ideal Rydberg backend.

The first step of our compilation is to map the Hilbert space of the target system to a subsystem of the ideal Rydberg backend. In our case, a site-to-site trivial mapping \mathcal{M} suffices. This may not always suffice for complicated cases, hence in general we need to search for a site mapping.

To synthesize H_{tar} , the SimuQ compiler enumerates product Hamiltonians (e.g., a singleton Z_1) of H_{tar} and searches for their presence in the Rydberg AAIS. The compiler builds an equation system by the coefficients of the product Hamiltonians, as illustrated in Figure 2 (the full equation system is presented in Appendix A). For instance, Z_1 appears in $H_{t_{\text{sys}}}$ and $H_{t_1, v_{t_1}}$, whose coefficients are

$$H_{t_{\text{sys}}} [Z_1] = -\frac{C}{4(x_1 - x_2)^6} - \frac{C}{4(x_1 - x_3)^6}, \quad H_{t_1, (\Delta_{t_1}, \Omega_{t_1}, \phi_{t_1})} [Z_1] = \frac{\Delta_{t_1}}{2}. \quad (2.2.10)$$

Here x_2 and x_3 are the global variables (x_1 is set to be 0) and Δ_{t_1} is the local variable of t_1 . To model whether this instruction is activated, we denote it by a switch variable $s_{t_1} \in \{0, 1\}$. Then the compiler builds an equation for Z_1 as

$$H_{t_{\text{sys}}} [Z_1] + H_{t_1} [Z_1] s_{t_1} = \mathcal{A}(H_{\text{tar}}) [Z_1] \Leftrightarrow -\frac{C}{4(x_1 - x_2)^6} - \frac{C}{4(x_1 - x_3)^6} + \frac{\Delta_{t_1}}{2} \cdot s_{t_1} = -\frac{1}{2}. \quad (2.2.11)$$

A mixed-binary non-linear equation solver is leveraged to obtain an approximate solution to the constructed equation system, with solutions presented in Figure 2. We now interpret the solution as an instruction schedule S on the ideal Rydberg backend. We set the atom positions by the valuation of x_1, x_2, x_3 . Notice $s_{t_1} = s_{t_2} = s_{t_3} = 1$, so all the instructions are activated during time $[0, 1]$. For the

$A \in \text{Site},$	$r \in \mathbb{R}, t \in \mathbb{R}^+$	$h_{A.R} = R_A$
$R \in \text{Operator}$	$::= I \mid X \mid Y \mid Z$	$h_{S.M} = \text{eval}(S) \cdot h_M,$
$S \in \text{Scalar}$	$::= S_1 + S_2 \mid S_1 \cdot S_2 \mid S_1 - S_2 \mid S_1/S_2$ $\mid \exp(S) \mid \cos(S) \mid \sin(S) \mid r$	$h_{M_1+M_2} = h_{M_1} + h_{M_2},$ $h_{M_1 \cdot M_2} = h_{M_1} \cdot h_{M_2},$
$M \in \text{Hermitian}$	$::= M_1 + M_2 \mid M_1 \cdot M_2 \mid S \cdot M \mid A.R$	$\llbracket \text{nil} \rrbracket = I,$
$P \in \text{Evolution}$	$::= \text{nil} \mid (M, t); P$	$\llbracket (M, t); P \rrbracket = \llbracket P \rrbracket \cdot e^{-ith_M}.$

(a) Syntax of HML.

(b) Semantics of HML programs.

Fig. 3. Syntax and denotational semantics of HML. Here Site contains system sites. h_M translates M into a Hermitian matrix. R_A is the Hermitian matrix where R applies to site A 's Hilbert space and I applies to the complement space. Function eval evaluates S to a real number.

i -th laser, we create constant functions over time with values Δ_{ℓ_i} , Ω_{ℓ_i} and ϕ_{ℓ_i} correspondingly as the parameter pulses.

We pass the solution schedule \mathcal{S} to (2.2.8), and obtain the synthesized Hamiltonian

$$H_{\text{Rydberg}}^{\mathcal{S}}(t) = -(1.03\hat{n}_1 + \hat{n}_2 + 1.03\hat{n}_3) + 2(X_1 + X_2 + X_3) + (4\hat{n}_1\hat{n}_2 + 4\hat{n}_2\hat{n}_3 + 0.06\hat{n}_1\hat{n}_3) \quad (2.2.12)$$

$$= \mathcal{A}(H_{\text{tar}}) + 0.016 \cdot (Z_1Z_3 - I). \quad (2.2.13)$$

The synthesis difference, $0.016 \cdot (Z_1Z_3 - I)$, is small, and we provide theoretical bounds on the evolution error induced by this difference in Section 4.2.

The SimuQ compiler generates a program for schedule \mathcal{S} in Bloqade language, a programming language designed for Rydberg atom systems. This pulse program can be executed on QuEra's neutral atom machines.

3 DOMAIN-SPECIFIC LANGUAGES

In order to depict the simulation problem and the backend machine, two domain-specific languages are proposed in our framework: Hamiltonian Modeling Language to model the quantum systems and dynamics and AAIS Specification Language to specify AAISs of machines.

3.1 Hamiltonian Modeling Language

In order to describe a target physical system in a lightweight and expressive way, we propose Hamiltonian Modeling Language (HML). Many novel abstractions are introduced in this language, including sites and site-based representations of Hamiltonians. We implement this language in Python, with its abstract syntax and denotational semantics defined formally in Figure 3.

Abstract Syntax of HML. We first introduce sites and their operators in the target system. A qubit site is a quantized 2-level physical entity, for example, atoms with 2 energy levels. In HML, site identifiers are collected in a set Site, each representing a site of the system. Four operators, I , X , Y , and Z , are defined to represent the Pauli operators, and they are used as site operators. We denote the X operator of qubit q as $q.X$ and the other operators in a similar way.

A time-independent Hamiltonian is effectively a Hermitian matrix and is programmed by algebraic expressions. The basic elements of expressions are site operators $A.R$ and scalars S . We collect the common operations between scalars in the definition of S . The operations between Hamiltonians correspond to the mathematical operations, whose physical meanings are introduced in Section 2.1.

$A \in \text{Site}$, $U \in \text{Property}$, $L \in \text{SigLine}$,	$h_{A,R} = R_A$,
$l \in \text{LocalVar}$, $g \in \text{GlobalVar}$, $r \in \mathbb{R}$	$h_{S,M} = \overline{\text{eval}}(S) \cdot h_M$,
$R \in \text{Operator}$	$h_{M_1+M_2} = h_{M_1} + h_{M_2}$,
$S \in \text{Para. Scalar}$	$h_{M_1 \cdot M_2} = h_{M_1} \cdot h_{M_2}$,
	$\{\text{nil}\} = \text{nil}$,
$M \in \text{Para. Hermitian}$	$\{M^{L,U}; P\} = (h_M, L, U); \llbracket P \rrbracket$
$P \in \text{Machine}$	
	(b) Semantics of AAIS programs.

(a) Syntax of AAIS specification language.

Fig. 4. Abstract syntax and denotational semantics of AAIS specification language. Here Site contains machine sites. Property contains instruction properties, including **nat**, **der**, and **sys**. SigLine contains the signal lines of the machine. LocalVar contains the local variables. GlobalVar contains the global variables. $\overline{\text{eval}}(S)$ evaluates S as a function taking the valuation of variables and generating a Hermitian matrix.

An evolution P then is programmed in HML as a sequence of pairs (M, t) of a time-independent Hamiltonian H programmed as M and its evolution time t . Such a sequence in P represents a sequential evolution under each H for time t , and overall, an evolution under a piecewise constant Hamiltonian. In many-body physics systems, Hamiltonians are commonly continuous. These Hamiltonians are discretized into a series of piecewise constant Hamiltonians by evaluating them over a discrete list of time, realized as syntactic sugars with user-specified precision and then programmed in HML. The error induced by discretization is analyzed in Section 4.2.

Semantics of HML. The denotational semantics of a program P in HML is interpreted as a unitary matrix by $\llbracket P \rrbracket$ in Figure 3b. We let h_M translate program M into Hermitian matrices by evaluating the expressions. Then $\llbracket P \rrbracket$ is the product of unitary matrices e^{-ith_M} , each representing the solution to the Schrödinger equation under $H(\tau) = h_M$ for time duration t . This is the solution to the Schrödinger equation of the piecewise constant Hamiltonian evolution represented by P .

3.2 Abstract Analog Instruction Set Specification Language

An abstract analog instruction set conveys the capability of a quantum device, which is essential machine information for the synthesis of target Hamiltonians. It contains abstract sites, the signal lines, and the possible instructions on each signal line. We propose AAIS Specification Language to depict them and present its abstract syntax and denotational semantics in Figure 4.

An AAIS contains site identifiers in Site to represent qubit sites, and site operators are defined in the same syntax in AAIS Specification Language as in HML. Quantum machines have tunable parameters. We design variables corresponding to the parameters on the real machine, divided into two types: global variables and local variables. Global variables are set before evolution and fixed for later simulations. Local variables are tunable for each constant Hamiltonian evolution. Variable identifiers are stored in LocalVar and GlobalVar in AAIS specification language. They are invoked in parameterized scalars and Hermitians, and their values will be filled during compilation.

In AAIS Specification Language, an instruction is effectively a parameterized Hermitian M decorated by the signal line L to which it belongs and its property U . Signal line identifiers are stored in SigLine, and each of them models a carrier of signals, the media for different kinds of analog signals sent to quantum devices. Instructions are broadly sorted into three categories: native, derived, and system instructions, and are distinguished by instruction properties $U \in \text{Property} = \{\text{nat}, \text{der}, \text{sys}\}$,

decorating the instructions. A native instruction corresponds to procedures with direct physical effects. It can be activated simultaneously with other instructions and superposes effects on the system. A derived instruction realizes an effective Hamiltonian H via an indirect reproduction of H , hidden from the AAIS. It may cross-talk with other instructions when they both influence one or more sites simultaneously, resulting in non-superposition effects. For some devices, there exists a non-negligible system Hamiltonian. We model it as a system instruction of a standalone system signal line, which can be activated simultaneously with other native instructions. We do not limit the governance of instructions over local variables in AAIS Specification Language, although in our applications a local variable only appears in one instruction. This difference does not affect our formal discussion, so we omit further discussions.

An analog machine is programmed as a list of instructions. These instructions fully describe the capabilities of a device and abstract away pulse implementation details. Because these underlying details are typically complex, the design and programming of an AAIS should be carried out by device developers.

Semantics of AAIS Specification Language. In Figure 4b, we interpret machines P in AAIS Specification Language via $\{\cdot\}$ into a list of instructions represented by a tuple consisting of Hamiltonian H , signal line L , and property U , which is sufficient for our SimuQ compiler to generate instruction schedules. The function $\text{eval}(\cdot)$ for AAIS Specification Language is an extension of $\text{eval}(\cdot)$ in HML, where $\text{eval}(S)$ represents a function taking a valuation of variables and generating a real number. A parameterized Hermitian M is translated into h_M , which is a function taking a variable valuation and generating a Hermitian. We abuse the notation by letting $\{\iota\} = h_M$ represent the parameterized Hermitian of instruction $\iota = M^{L,U}$.

4 SIMUQ COMPILER

Compiling a target quantum system to an analog quantum device is computationally hard in most cases, especially when we aim at a general framework. In this section, we build the first compiler for quantum simulation on general analog quantum devices. The compiler generates an instruction schedule and a site mapping, such that the target system is reproduced on the device’s subsystem specified by the site mapping. Then the compiler translates the instruction schedule to executable pulses for quantum devices.

Since this is the first exploration of compilation to general analog devices, our proposal intuitively decomposes the problem into several natural steps and then applies straightforward solutions to each step. Much space for optimizing our workflow within the scope of our approach is left for future work, which is discussed in Section 6.

4.1 Compilation to Instruction Schedules

4.1.1 Instruction Schedules. An instruction schedule S describes what a machine executes at a given time. Formally, $S(L, t) = (\iota, v)$ displays the instruction ι to carry for signal line L at time t and a valuation v of variables. If signal line L carries no instruction at time t , we write $S(L, t) = \perp$. We then formally define the validity of an instruction schedule.

DEFINITION 4.1. *We denote the influencing sites of M as $\text{inf}(M)$, defined by*

$$\begin{aligned} \text{inf}(S \cdot M) &= \text{inf}(M), & \text{inf}(A.R) &= \{A\}, \\ \text{inf}(M_1 + M_2) &= \text{inf}(M_1) \cup \text{inf}(M_2), & \text{inf}(M_1 * M_2) &= \text{inf}(M_1) \cup \text{inf}(M_2). \end{aligned}$$

Two instructions $\iota_1 = M_1^{L_1, U_1}$ and $\iota_2 = M_2^{L_2, U_2}$ conflict with each other either if $L_1 = L_2$, or if $\text{inf}(\iota_1) \cap \text{inf}(\iota_2) \neq \{\}$ and $\text{der} \in \{U_1, U_2\}$.

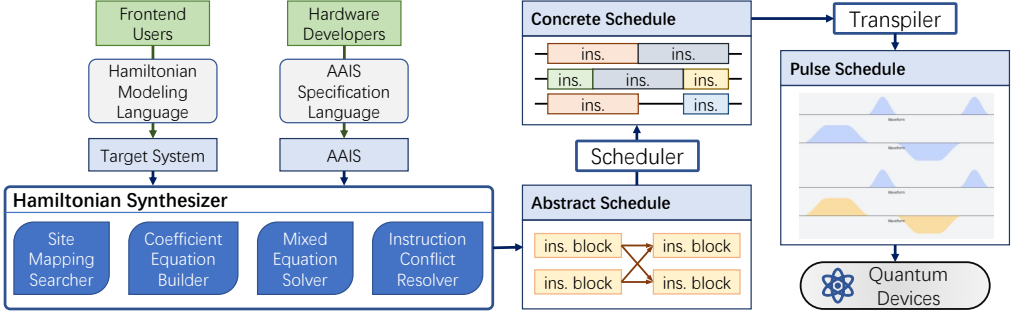


Fig. 5. The framework of SimuQ.

An instruction schedule S is invalid if two conflicting instructions are activated simultaneously. Formally, for a valid S , any t and $L_1 \neq L_2$, let $S(L_1, t) = (M_1^{L_1, \text{der}}, v_1)$ and $S(L_2, t) = (M_2^{L_2, U_2}, v_2)$, there is $\text{inf}(M_1) \cap \text{inf}(M_2) = \{\}$.

In this paper, we assume that any derived instruction $\iota = M_1^{L_1, \text{der}}$ does not have any side effect: it does not cross-talk with another instruction $\iota' = M_2^{L_2, U}$ where $\text{inf}(M_1) \cap \text{inf}(M_2) = \{\}$.

4.1.2 Hamiltonian Synthesizer. We consider the synthesis of a time-independent Hamiltonian H_{tar} evolving for time duration T given a machine AAIS $\iota_1; \dots; \iota_m$. Our Hamiltonian synthesizer follows a four-step process: (1) find a site mapping \mathcal{A} ; (2) build a coefficient equation system; (3) solve the mixed-binary equation system; (4) resolve conflicting instructions.

Site mapping searcher. A brute-force search with pruning is applied to find a site mapping \mathcal{A} from the target system sites to the machine sites. We write $\mathcal{A}(H)$ for Hamiltonian H under mapping \mathcal{A} . We prune the search by enforcing that, for product Hamiltonian P such that $H_{\text{tar}}[P] \neq 0$, there exists $1 \leq j \leq m$ such that $\{\iota_j\}[\mathcal{A}(P)] \neq 0$. The aborting condition can be met halfway in the search, where $\mathcal{A}(P)$ does not exist in the machine when limited to the already-searched sites. Whenever the search completely constructs a site mapping, we continue to the next steps and check the feasibility of this site mapping. If an instruction schedule is found, the compilation succeeds. If none of the searched site mappings are feasible, the compiler reports no possible solution.

Coefficient equation builder. We synthesize instructions and valuations to variables to realize H_{tar} by building and solving a system of mixed-binary non-linear equations. We create a switch variable $s_i \in \{0, 1\}$ for instruction ι indicating if ι is activated. For each product Hamiltonian P in $\mathcal{A}(H_{\text{tar}})$ and $\{\iota_j\}$, we build an equation

$$\sum_{j=1}^m \{\iota_j\}[P] \cdot s_{\iota_j} = \mathcal{A}(H_{\text{tar}})[P]. \quad (4.1.1)$$

For a system Hamiltonian ι_{sys} , we set $s_{\iota_{\text{sys}}} = 1$. We propose a heuristic algorithm Algorithm 1 to find all non-trivial equations (where $\mathcal{A}(H_{\text{tar}})[P] \neq 0$ or no instruction ι such that $\{\iota\}[P] \neq 0$ may activate). This algorithm starts with a list Q containing all the product Hamiltonians that may correspond to a non-trivial equation. At first, it contains every product Hamiltonian in $\mathcal{A}(H_{\text{tar}})$ if the coefficient is non-zero. We then enumerate the list Q and establish coefficient equations for each product Hamiltonian in Q by enumerating every instruction in AAIS. During this process, we may encounter instruction Hamiltonians who contain product Hamiltonians that never appear in Q . These product Hamiltonians are also non-trivial, so we add them to Q . Specifically, for the

Algorithm 1 Heuristic equation builder for Hamiltonian synthesis.

Inputs: site mapping \mathcal{A} , target H_{tar} , AAIS $\mathcal{M} = \{\iota_j = M_j^{L_j, U_j}\}_{j=1}^K$

Output: a system of equations Υ .

```

 $Q \leftarrow \{P \mid \mathcal{A}(H_{\text{tar}})[P] \neq 0\}$ 
 $\Upsilon \leftarrow \{\}$ 
 $i \leftarrow 0$ 
while  $i < |Q|$  do
   $P \leftarrow Q[i]$ 
  if  $P = I$  then
     $i \leftarrow i + 1$ 
    continue
   $e \leftarrow 0$ 
  for  $\iota \in \mathcal{M}$  do
    if  $\{\iota\}[P] \neq 0$  then
       $e \leftarrow e + \{\iota\}[P] \cdot s_i$ 
      for  $J : \{\iota\}[J] \neq 0, J \neq P$  do
        if  $J \notin Q$  then
           $Q.append(J)$ 
       $\Upsilon.add(e = \mathcal{A}(H_{\text{tar}})[P])$ 
     $i \leftarrow i + 1$ 
  for  $\iota \leftarrow M^{L,U} \in \mathcal{M}$  do
    if  $U = \text{sys}$  then
       $s_i \leftarrow 1$ 
      for  $P : \{P \mid \{\iota\}[P] \neq 0\}$  do
        if  $P \notin Q$  then
           $\Upsilon.add(\{\iota\}[P] = 0)$ 

```

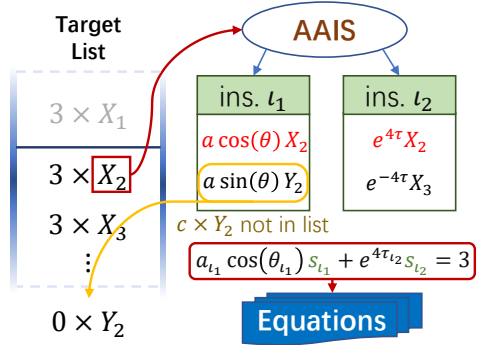


Fig. 6. An example illustrating the equation builder. X_2 is searched for in AAIS, where ι_1 and ι_2 are found and used in equation construction for X_2 .

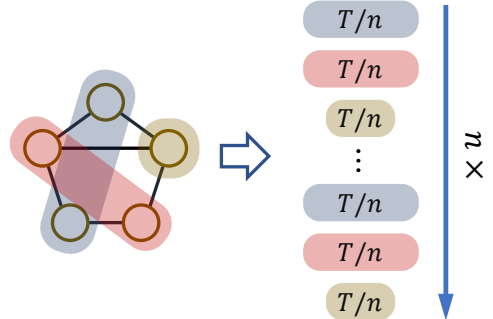


Fig. 7. An example of a conflict graph, its no-conflict grouping, and an instruction schedule after Trotterization.

system instruction, since it is always on, we force the terms not appearing in Q to have coefficients equaling to 0. An example of this procedure is illustrated in Figure 6. For any instruction ι not appearing in this procedure, we force $s_i = 0$.

Mixed equation solver. Because there is no general-purpose solver for mixed-binary non-linear equations, we hand-crafted a small solver. Our solver uses a relaxation-rounding scheme. We apply a continuous relaxation to loosen the value range of switch variables from $\{0, 1\}$ to $[0, 1]$ and solve the equation system by least square methods using a finite-difference scheme via an implementation in SciPy. We then round the switch variables according to the solution. Because many instructions contain an amplitude variable as a multiplier to the Hamiltonian, we round switch variable s to 1 if $\text{abs}(s) > \delta$ for a pre-defined small threshold δ and set $s = 0$ otherwise. We then try to solve the equation system again with fixed switch variables to determine the valuation of global and local variables. The solution directly corresponds to the instructions to activate ($s_i = 1$) and the valuation of variables. Using the least square solver, we can also restrain the variables with lower and upper bounds and set proper initial values. If no solution within an error threshold is found, we return to the site mapping search and report \mathcal{A} infeasible.

Instruction conflict resolver. Lastly, we resolve conflicting instructions. By Definition 4.1, we can build a conflict graph $C = (V, E)$ where $V = \{\iota \mid s_i = 1\}$ and $E = \{(\iota_i, \iota_j) \mid \iota_i \text{ conflicts with } \iota_j\}$. We then divide V into S subsets U_1, \dots, U_S where $E|_{U_i} \triangleq \{(\iota_1, \iota_2) \mid \iota_1, \iota_2 \in U\} = \{\}$ for any i . This is effectively a graph vertex coloring problem, and we employ a greedy graph coloring algorithm from NetworkX to find a feasible division. Notice that for each U_i , there is no conflicting instruction pair, so one can construct a valid instruction schedule $\mathcal{S}_{U_i, t}$ to evolve under $H_{U_i} = \sum_{\iota \in U_i} H_{(\iota, v)}$ for time duration t . We then apply Trotterization (also known as the product formula algorithm), a common technique in quantum information, to approximate the required evolution under $H_{\text{tar}} = \sum_{i=1}^K H_{U_i}$ by sequentially evolving under H_{U_i} . According to the Lie-Trotter formula

$$e^{\sum_j A_j} = \lim_{n \rightarrow \infty} \left(\prod_j e^{A_j/n} \right)^n, \quad (4.1.2)$$

we divide the total evolution time T into n pieces, where n is the Trotterization number pre-defined by users. We sequentially evolve H_{U_i} for time duration T/n and repeat this process n times. Let $\mathcal{S}_1 \rightarrow \mathcal{S}_2$ represent the instruction schedule obtained by appending \mathcal{S}_2 after \mathcal{S}_1 . A valid instruction schedule approximating the evolution of H_{tar} for duration T is characterized by

$$\mathcal{S} = (\mathcal{S}_{U_1, T/n} \rightarrow \dots \rightarrow \mathcal{S}_{U_S, T/n}) \rightarrow \dots \rightarrow (\mathcal{S}_{U_1, T/n} \rightarrow \dots \rightarrow \mathcal{S}_{U_S, T/n}), \quad (4.1.3)$$

which combines n repetitions of the instruction schedule simulating H_{U_i} for duration T/n sequentially for $1 \leq i \leq S$. Ideally, when n tends to infinity, the evolution is perfectly simulated. Practically, n should not be too large because of overhead costs in the instruction implementation.

REMARK 4.1. *At the start of compilation, a continuous Hamiltonian $H(t)$ is discretized into a piecewise constant Hamiltonian. For multiple pieces of evolution, the SimuQ compiler deals with them sequentially using the above procedures. Notice that for each piece, the local variables and switch variables have new copies specified for this piece. However, they share the same set of global variables in the coefficient equation system since global variables are fixed before the evolution starts.*

REMARK 4.2. *In general, compiling a target system is computationally hard. For machines with specific topology, finding a site mapping can be as hard as the sub-graph isomorphism problem, an NP-complete problem. Besides, since in the design of AAIS we do not pose strict restrictions on the expression, pathological functions may emerge in the coefficient of product Hamiltonian terms, which complicates the equation-solving process. Our solutions to these problems are not optimal, but feasible and efficient enough for most cases (also refer to Section 5.4 for detailed case studies).*

4.2 Soundness of Compilation to Instruction Schedules

If the compilation process succeeds in compiling evolution under $H_{\text{tar}}(t) = \sum_{k=1}^K \alpha_k(t) H_k$ for duration T , the SimuQ compiler generates a site mapping \mathcal{A} and a schedule \mathcal{S} approximating evolution under $\mathcal{A}(H_{\text{tar}}(t))$. We analyze the approximation errors between the target and synthesized evolution (represented by unitary matrices) produced in the discretization procedure and the compilation procedure. The errors come from discretization, the equation solver, and Trotterization, and the errors decrease when we increase the discretization number, improve the compilation solver, or increase the Trotterization number, respectively, implying the soundness of our compilation process.

4.2.1 Error induced by Discretization. We apply a piecewise constant discretization of $H_{\text{tar}}(t)$ to $\tilde{H}(t) = \sum_{k=1}^K \tilde{\alpha}_k(t) H_k$. We assume that $\alpha_k(t)$ are piecewise L -Lipschitz functions. Let the evolution duration be T and the discretization number be D . Formally,

$$\tilde{\alpha}_k(t) = \sum_{j=0}^{D-1} \tilde{\alpha}_{k,j} \mathbb{1}_{[\frac{T}{D} \cdot j, \frac{T}{D} \cdot (j+1))}(t), \quad \tilde{\alpha}_{k,j} = \tilde{\alpha}_k(j \cdot T/D), \quad (4.2.1)$$

where $\mathbb{1}_{[a,b]}$ is the indicator function of set $[a, b]$.

LEMMA 4.2 ([HAYES ET AL. 2014]). *The difference between the unitary $U(T)$ of evolution under $\mathcal{A}(H_{\text{tar}}(t))$ for duration T and the unitary $\tilde{U}(T)$ of evolution under $\mathcal{A}(\tilde{H}(t))$ is bounded by*

$$\|U(T) - \tilde{U}(T)\| \leq C_1 D^{-1} L K T^2 \triangleq \mathcal{E}_1. \quad (4.2.2)$$

Here $\|\cdot\|$ is the spectral norm of matrices, $C_1 > 0$ is a constant, D is the discretization number, and L is the Lipschitz constant for $\alpha_k(t)$, K is the number of terms in $H(t)$, T is the evolution duration.

This lemma shows that when we increase the discretization number D , the evolution error can be arbitrarily small, justifying our method of discretization. The proofs to these lemmas are routine in quantum information, and we omit them here.

4.2.2 Error induced by the Equation Solution. In the SimuQ compiler, we use a mixed-binary equation solver to synthesize piecewise constant $\tilde{H}(t)$. Since the solution is numerical, errors in the evolution are induced by errors in the synthesis. Let the synthesis result be $\hat{H}(t)$. Notice that each equation built from Algorithm 1 effectively is $\hat{H}(t)[P] = \mathcal{A}(\hat{H}(t))[P]$ for each piece and each product Hamiltonian P , and we conclude the following lemma.

LEMMA 4.3 ([HAYES ET AL. 2014]). *If the compilation procedure succeeds, the difference between the unitary $\tilde{U}(T)$ and the unitary $\hat{U}(T)$ of evolution under $\hat{H}(t)$ is bounded by*

$$\|\tilde{U}(T) - \hat{U}(T)\| \leq C_2 \Delta E T \triangleq \mathcal{E}_2. \quad (4.2.3)$$

Here $C_2 > 0$ is a constant, $\Delta = \max_{t,P} \|\hat{H}(t)[P] - \mathcal{A}(\tilde{H}(t))[P]\|$ is the error of the equation solution, E is the number of equations built from Algorithm 1, and T is the evolution duration.

If the solver finds a precise solution, the error in this step decreases.

4.2.3 Error induced by Trotterization. The Trotterization technique resolves conflicts while also introducing errors. For the constant piece of \hat{H} at time slice t , we divide the activating instructions into S_t groups without conflicts, realizing $\check{H}_{t,i}$ such that $\sum_{i=1}^{S_t} \check{H}_{t,i} = \hat{H}(t)$. When the Trotterization number is set to N , the system evolves under each group for duration $\frac{T}{DN}$ sequentially with arbitrary order and repeats this procedure N times.

LEMMA 4.4 ([CHILDS ET AL. 2018]). *The difference between $\hat{U}(T)$ and the unitary $\check{U}(T)$ of evolution after Trotterization is bounded by*

$$\|\hat{U}(T) - \check{U}(T)\| \leq \frac{(\Lambda T)^2}{DN} e^{\frac{\Lambda T}{DN}} \triangleq \mathcal{E}_3. \quad (4.2.4)$$

Here $\Lambda = \max_t S_t \|\check{H}_{t,i}\|$, T is the evolution duration, D is the discretization number, and N is the Trotterization number.

As implied by this lemma, increasing the Trotterization number reduces the induced error, and the error can be arbitrarily small.

4.2.4 Total Error in Compilation. Combining the above three lemmas via the union bound, we conclude the following theorem bounds the total error, implying the soundness of our compilation: if the mixed equation solver finds a precise solution and the discretization and Trotterization numbers are sufficiently large, ideally, the generated instruction schedule simulates $H_{\text{tar}}(t)$.

THEOREM 4.5. *The error in SimuQ compilation is bounded by $\|U(T) - \check{U}(T)\| \leq \mathcal{E}_1 + \mathcal{E}_2 + \mathcal{E}_3$.*

4.3 Implementing Instruction Schedules

Because the underlying pulse implementation of an instruction evolving for duration t in \mathcal{S} does not necessarily have length t and may break synchronicity, we implement instruction schedules \mathcal{S} more flexibly. We propose abstract schedules that include the valuation of the variables and the temporal relations between blocks of instruction, relaxing the fixed time slot of instruction calls in instruction schedules. The AAIS of the machine is exposed to abstract schedules, but concrete instruction implementations are implicit.

The basic unit of an abstract schedule is an instruction block containing an evolution time t and non-conflicting instructions with the valuation of their local variables. The instructions in a block are intended to simultaneously activate for duration t .

The temporal relations form a directed acyclic graph whose vertices are the instruction blocks. An edge $(i \rightarrow j)$ represents a restraint: the block j start after the execution of block i . One may extract instruction schedules from an abstract schedule by scheduling the instruction blocks according to the temporal relations, and they approximate the target quantum system by Theorem 4.5.

4.4 Scheduling Instruction Calls

A concrete schedule is a time schedule specifying the starting and ending time of each instruction call on the real machine. Determining exact timing necessitates instruction implementation details, and the compiler, therefore, requires backend machine details. We accomplish this by using a platform-dependent machine object to convert each instruction call into an equivalent schedule block object specifying the exact instruction execution duration on the real machine. We then use a simple scheduler to produce a concrete schedule from the directed acyclic graph of schedule blocks. Our scheduler traverses the DAG in topological order and schedules each instruction for execution on the appropriate machine signal line at the first available time slot. Visiting each schedule block in topological order ensures that signal line reservations are made in a valid temporal order, and our greedy scheduling approach ensures that the execution order fulfills all temporal dependencies.

REMARK 4.3. We note that this scheduling process may be independently configured and optimized, and the scheduler may use any number of other criteria to determine the traversal order of instruction blocks or the alignment of blocks within the scheduled order. This freedom in the scheduling process may be leveraged to reduce cross-talk between the blocks or save basis change overhead. We illustrate a basic strategy in this paper and leave the exploitation to future works.

4.5 Transpilation to Pulses

In its final stage, our end-to-end framework transpiles a concrete schedule into a generalized pulse program and produces an equivalent platform-dependent executable pulse program. A generalized pulse program stores a control pulse for a given signal line as a list of variable waveforms. Each waveform tracks the time evolution of controllable local variables specified by instructions on that signal line. We then leverage a platform-dependent machine object to convert a generalized pulse program into a format specified by a pulse-enabled quantum device provider for execution on a real machine.

There are few pulse-enabled quantum device providers, and programming pulses is a challenging endeavor that requires extensive platform knowledge of a variety of hardware and software engineering considerations. Nonetheless, we demonstrate the effectiveness of our framework using both QuEra’s Bloqade [QuEra 2022] and IBMQ’s Qiskit Pulse [Alexander et al. 2020], and we note that for generality, SimuQ supports output as a quantum circuit.

For QuEra’s machine, our generalized pulse schedules are converted to Bloqade programs. Our magnitude variable waveforms and atom position global variables have native correspondences to

the values specified in control pulses and control parameters sent to the machine, so the conversion is performed trivially.

On IBM devices, our generalized pulse schedules are converted to Qiskit Pulse programs. We use our magnitude variable waveforms to build signal envelopes for control pulses sent to the device and insert software-implemented “free Z” rotations at time indices where our phase variable waveforms change in value. Furthermore, because Qiskit Pulse [Alexander et al. 2020] supports pulse-level engineering and provides more freedom than the IBM native gate set, our pulse programs may be constructed from more optimized operations and produce shorter pulse programs than Qiskit’s default compilation. In particular, we engineer better pulse realizations of evolution under $X_i X_j$, $Y_i Y_j$, and $Z_i Z_j$, and we discuss the details further in Section 5.2.

Since IonQ does not provide pulse-level programmability for their ion trap devices, so we generate quantum circuits with rotation gates $R_X, R_Z, R_{XX}, R_{YY}, R_{ZZ}$ and send these circuits to IonQ’s compilers and devices. For example, the evolution of under $X_i X_j$ for duration T is realized by $R_{XX}(2T)$ applying on qubits i and j .

5 CASE STUDIES

We implement Hamiltonian modeling language and AAIS specification language in Python and program quantum models and quantum devices with pulse control, as in Figure 8. We conduct several case studies on these evolutions and devices to highlight SimuQ’s portability, pulse performance, flexibility, and scalability.

```
MIS = QSystem()
q = [qubit(MIS) for i in range(N)]
n = [(q[i].I - q[i].Z) / 2 for i in range(N)]
Σn = sum([n[i] for i in range(N)])
ΣX = sum([(q[i].X for i in range(N)])
Σnn = sum([n[i] * n[j] for (i, j) in E])
def H(t) :
    return (-(-1 + 2 * t / T) * U * Σn
            + ω / 2 * ΣX + α * Σnn)
MIS.add_td_evo(H, T, D)
```

(a) The MIS Hamiltonian. N is the number of sites. U and α are Hamiltonian parameters. T is the time duration. E contains the graph topology. D is the discretization number.

```
QAOA = QSystem()
q = [qubit(QAOA) for i in range(N)]
ΣZZ = sum([q[i].Z * q[j].Z for (i, j) in E])
ΣX = sum([X[i] for i in range(N)])
for i in range(p) :
    QAOA.add_evo(θ[i] * ΣZZ, 1)
    QAOA.add_evo(y[i] * ΣX, 1)
```

(b) The QAOA evolution. N is the number of sites. θ and y are QAOA parameter lists. E contains edges of the target graph.

```
Heis = QSystem()
q = [qubit(Heis) for i in range(N)]
ΣXX = sum([q[i].X * q[i+1].X for (i, j) in E])
ΣYY = sum([q[i].Y * q[i+1].Y for (i, j) in E])
ΣZZ = sum([q[i].Z * q[i+1].Z for (i, j) in E])
ΣZ = sum([q[i].Z for i in range(N)])
h = Jx * ΣXX + Jy * ΣYY + Jz * ΣZZ + c * ΣZ
Heis.add_evo(h, T)
```

(c) The Heisenberg Hamiltonian. N is the number of sites. J_x , J_y , J_z , c are Hamiltonian parameter. E stores graph topology. T is the time duration.

```
Rydberg = QMachine()
q = [qubit(Rydberg) for i in range(N)]
n = [(q[i].I - q[i].Z) / 2 for i in range(N)]
x = [0] + [GlobalVar(Rydberg) for i in range(1, N)]
h = sum([(C / (x[i] - x[j])**6) * n[i] * n[j]
         for i in range(N) for j in range(i)])
Rydberg.set_sys_ham(h)
i = Instruction(SignalLine(Rydberg), 'native')
Δ, Ω, φ = LocalVar(i), LocalVar(i), LocalVar(i)
hi = 0
for i in range(N) :
    hi += -Δ * n[i]
    hi += Ω / 2 * (cos(φ) * q[i].X - sin(φ) * q[i].Y)
i.set_ham(hi)
```

(d) An AAIS for QuEra’s machines. N is the number of sites. C is the Rydberg interaction constant.

```
Machine = QMachine()
q = [qubit(Mac) for i in range(N)]
Ins, LVar = Instruction, LocalVar
for i in range(N) :
    L = Signalline(Machine)
    i1, i2 = Ins(L, 'native'), Ins(L, 'derived')
    α1, φ, α2 = LVar(i1), LVar(i1), LVar(i2)
    i1.set_ham(α1 * (cos(φ) * q[i].X + sin(φ) * q[i].Y))
    i2.set_ham(α2 * q[i].Z)
for (i, j) in E :
    L = Signalline(Machine)
    [i1, i2, i3] = [Ins(L, 'derived') for k in range(3)]
    α1, α2, α3 = LVar(i1), LVar(i2), LVar(i3)
    i1.set_ham(α1 * q[i].X * q[j].X)
    i2.set_ham(α2 * q[i].Y * q[j].Y)
    i3.set_ham(α3 * q[i].Z * q[j].Z)
```

(e) An AAIS for IBM’s machines or IonQ’s machines. Here E is the number of sites. For IBM’s machines, E stores the machine topology. For IonQ’s machines, E contains every pair between sites.

Fig. 8. HML and AAIS specification language programs in Python for case studies.

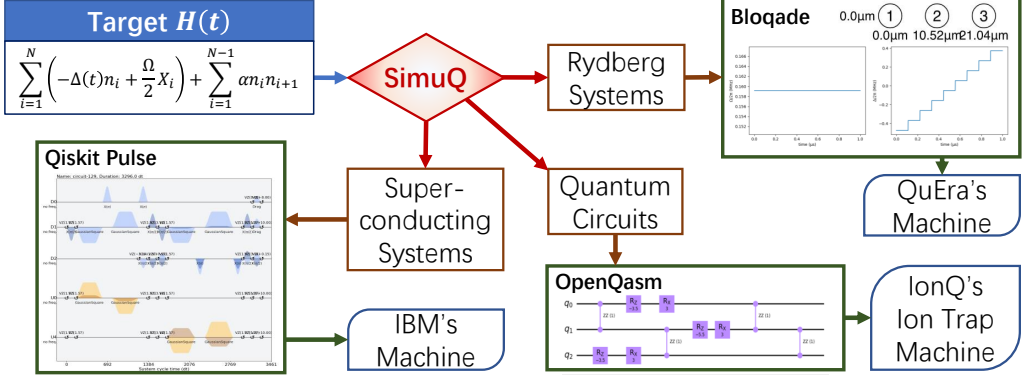


Fig. 9. Compiling a Hamiltonian to multiple platforms via SimuQ.

In our implementation, we treat time-independent Hamiltonians in *standard forms* – linear combinations of product Hamiltonians. Expressions of Hamiltonians can be expanded by the distributive laws, and eventually into the standard form. Hamiltonians are stored in a Python list of pairs consisting of product Hamiltonians and coefficients. Product Hamiltonians are realized as tuples of operators on each site. We symbolically realize the algebraic operations between Hamiltonians, so users program Hamiltonians via operations like addition and multiplication conventionally. For parameterized scalars in AAIS specification language, we build an Expression class to deal with the calculus of functions of valuations of local and global variables, and they work as coefficients of product Hamiltonians for parameterized Hermitians.

5.1 Compilation to Multiple Platforms

We compile a target Hamiltonian to multiple platforms, including QuEra’s Rydberg atom arrays, IBM’s transmon qubit systems, and IonQ’s trapped ion systems. Their AAISs follow our discussion in Section 2.2.3, with slight differences to match current machines, and are displayed in Figure 8d and Figure 8e. The details of their AAIS design are discussed in Appendix B.

We return to the target Hamiltonian introduced in Section 2.2.1. It is a simplified Hamiltonian encoding of the maximal independent set (MIS) problem. For a graph $G = (V, E)$, the MIS problem asks for the maximal subset V' of V such that no edges in E connect two vertices in V' . According to [Ebadi et al. 2022], this problem can be encoded in the evolution initiated at $|0\rangle$ under the Hamiltonian

$$H_{\text{MIS}}(t) = \sum_{i=1}^N \left(-\delta(t) \hat{n}_i + \frac{\omega}{2} X_i \right) + \sum_{(i,j) \in E} \alpha \hat{n}_i \hat{n}_j \quad (5.1.1)$$

for $N = |V|$, time interval $[0, 1]$, and $\delta(t) = (-1 + 2t)U$. Here U , ω , and α are real amplitude constants designed in the encoding [Ebadi et al. 2022]. The measurement result of the quantum state at the end of the evolution encodes an approximate maximum independent set of the graph (after post-processing).

We instantiate this model on a chain of three vertices and set $U = 1$ and $\omega = \alpha = 4$. We program it in Python, displayed in Figure 8a, and compile it to different machines. The results on classical simulators are presented in Figure 10.

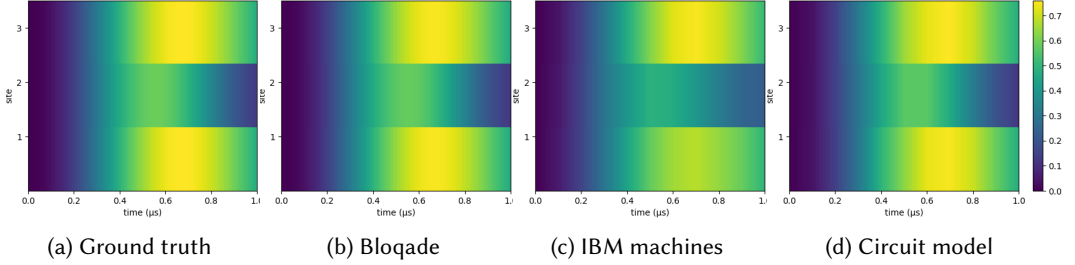


Fig. 10. Simulated evolution results of compilation to different platforms. It shows the probability of obtaining an excited state ($|1\rangle$) on each site when measured at different times, where the system evolves under H_{MIS} with $U = 1$, $\Omega = \alpha = 4$ for time interval $[0, 1]$, starting from state $|000\rangle$. The discretization number of the compilation is set to 10. (a) Ground truth evolution (no discretization). (b) Simulated evolution compiled to Rydberg platforms using Bloqade language and executed by the Bloqade simulator. (c) Simulated evolution compiled to IBM Qiskit and executed by a noisy IBM machine simulator modeling `ibmq_jakarta`. The Trotterization number is set to 1 to reduce the effects of noise. The probability is linearly interpolated using data points measured on every site and every $0.1\mu\text{s}$. (d) Simulated evolution compiled to quantum circuits, executed via an ideal circuit simulator, and linearly interpolated from the discretization. The Trotterization number is set to 10.

We consider the relative errors when compiling H_{MIS} on each device. The summed error is the summation of differences over the histogram in the simulation to the ground truth, and the relative error is the summed error over the sum of entries in the ground truth histogram. Since H_{MIS} has a very similar structure to the Rydberg system Hamiltonian, the compiled simulation is very close to the ground truth, with a 1.14% relative error. For IBM machines, the simulation is discrete since the instructions are derived. The discretization and machine noises induce significant differences from the ground truth probability, with an 8.30% relative error. We also compile the Hamiltonian to quantum circuits, setting the Trotterization number to 10. With an ideal simulator, the relative error is 1.67%. The results from all platforms are close to the ground truth; however, the simulation results may have larger errors on real devices where noise is significant.

5.2 Pulse-Oriented Optimized Compilation

We demonstrate that bypassing the gate abstraction guides us to prioritize reducing total pulse duration. IBM’s Qiskit has a circuit compiler that supports rotation gates realizing evolutions under both Z_iZ_j and X_i and can construct the evolution U . Their compilation translates a Z_iZ_j rotation gate into multiple single-qubit rotations and two cross-resonance gates, incurring a large overhead cost. To reduce total pulse duration, we implement evolution under Z_iZ_j with a dynamic duration cross-resonance evolution surrounded by single-qubit gates performing a basis change. This approach generates a significantly shorter pulse than Qiskit’s compilation, particularly when the desired evolution time is short. As shown in Figure 12, for evolution under Z_0Z_1 for duration 1, the pulse generated by SimuQ is 51% shorter in duration than the pulse generated by Qiskit’s compiler. Though the single gate fidelity may decrease, this approach is beneficial when a program requires a large number of short evolution instructions, as it can dramatically lower the total program duration and thereby mitigate decoherence over time. We illustrate this with an experiment using a quantum approximate optimization algorithm (QAOA) to solve the Max-Cut problem.

The Max-Cut problem asks for a separation V' of an unweighted graph $G = (V, E)$ such that the edges between V' and $V \setminus V'$ are maximized. By quantum annealing, alternately simulating the evolution of the initial state $|+\rangle^n$ under $\theta_j H_1$ and $\gamma_j H_2$ for fixed duration may generate solutions to

Layer	Qiskit	SimuQ
1	11328	4064
2	22656	9344
3	33984	15232

Table 2. Pulse duration (unit: dt) of QAOA evolution when compiling with Qiskit compiler and SimuQ. Here dt=0.22ns.

Layer	Qiskit	SimuQ	Ideal
1	8.145	8.2755	9
2	8.0705	8.635	10
3	7.3335	8.418	10.5

Table 3. Measured cut size of execution on real machines with pulses generated by Qiskit compiler and SimuQ. Ideal sizes are the expected cut size using the optimal parameters in QAOA.

	Current	Hypothetical
QAOA	15232	5056
Heisenberg	58944	19776

Table 4. Pulse duration (unit: dt) of current and hypothetical machines on QAOA evolution and the Heisenberg model. dt= 0.22ns.

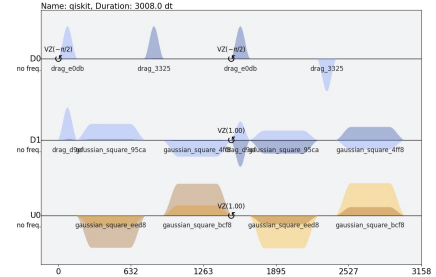


Fig. 11. Pulses generated by Qiskit compiler for evolution under Z_0Z_1 for duration 1. The pulse duration is 3158dt.

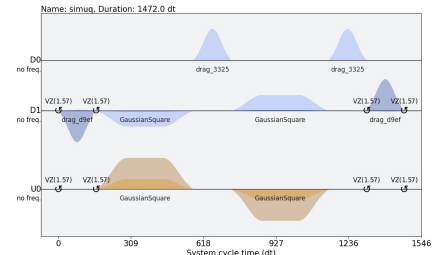


Fig. 12. Pulses generated by SimuQ for evolution under Z_0Z_1 for duration 1. The pulse duration is 1546dt.

the Max-Cut problem, where

$$H_1 = \sum_{(i,j) \in E} Z_i Z_j, \quad H_2 = \sum_{i=1}^N X_i. \quad (5.2.1)$$

Here $\{\theta_j\}_{j=1}^p$ and $\{\gamma_j\}_{j=1}^p$ are pre-defined parameters from the algorithm, and $N = |V|$. This procedure is programmed in Figure 8b. QAOA searches for the optimal evolution durations θ and γ to maximize the expected cut size $R(s) = \sum_{(i,j) \in E} [s_i \neq s_j]$, where s is the measurement outcome at the end.

We instantiate the problem with a 12-vertex cycle graph, layer $p = 1, 2, 3$, and θ, γ set to optimal parameters found by a classical simulator. We then compile this problem to IBM's machine executable pulses directly using SimuQ. Similarly, we reproduce this problem in Qiskit and compile it with the Qiskit compiler. In Table 2, we present a comparison of the duration of pulses produced by each method. Our solution significantly reduces the pulse duration with an average 59% reduction. We then execute the pulse programs produced by both methods on IBM's real machine, and present the measured cut sizes in Table 3. We observe that on average, SimuQ pulses produce errors 22% less often than Qiskit pulses. This demonstrates SimuQ's performance advantage and the necessity of pulse-oriented compilation.

5.3 Hypothetical Machines

SimuQ can also be leveraged to suggest the future design of machine functionalities because of its flexibility in supporting new machines. For example, if we have a hypothetical machine that supports native instructions like $X_i X_j$, $Y_i Y_j$, or $Z_i Z_j$ (meaning that these instructions can be applied

simultaneously), what advantage can we achieve for specific simulations? This question can be easily answered by SimuQ.

We create a hypothetical machine in correspondence with IBM's superconducting machine whose AAIS matches that of IBM's machine but with all instructions made native. Since $X_i X_j$, $Y_i Y_j$, and $Z_i Z_j$ are hypothetically assumed native, we may simultaneously apply these instructions, even when multiple instructions affect the same site. Furthermore, they require no change of basis operations in their implementation and pulse realization.

In Table 4, we show that the pulse duration of our QAOA example from Section 5.2 is reduced by 66.8%, suggesting the benefits of designing such instructions. To further illustrate the benefits of these hypothetical native instructions, we compile the Heisenberg model,

$$H_{\text{Heis}} = \sum_{(i,j) \in E} (J_x X_i X_j + J_y Y_i Y_j + J_z Z_i Z_j) + \sum_{i=1}^N c Z_i. \quad (5.3.1)$$

Here, J_x , J_y , J_z , and c are parameters modeling magnetic interactions, and E is a graph topology. We instantiate this model on a graph matching the machine topology of a 7-qubit IBM machine and compile it to both the real and hypothetical machines. Our results, presented in Table 4, show that the pulse duration on the hypothetical machine is reduced by 66.4%.

5.4 Scalability Test

We study the scalability of our SimuQ compiler by compiling many models of different sizes, topology, and discretization numbers, and we present our findings in Table 5 and Table 6. The following experiments were run on a laptop with an Intel i7-8705G CPU, and each reported time is an average of 5 repetitions.

There is no prior work to serve as a baseline on end-to-end software compiling a general many-body Hamiltonian simulation problem to machine executable programs. The hardness of this task mainly stems from four aspects. First, searching for a site mapping requires a subgraph isomorphism, an NP-complete problem asking for a subgraph in the machine topology graph matching the topology of the target Hamiltonian. Second, many quantum physics effects have highly non-linear dependencies on the controllable parameters, making the Hamiltonian synthesis hard. Third, the generality to compile all kinds of Hamiltonians unavoidably requires a large number of equations built for synthesis. Lastly, there are often many configurable parameters on a machine, creating a huge search space. Although the task is hard, for many problems in our applications, our SimuQ compiler succeeds in a reasonable time, automatically generating executable pulses in several minutes. However, there are still hard cases that SimuQ fails to tackle. There are three types of failures in our experiments. The first is no solution to find the target Hamiltonian to the device, reported after enumerating all possible options by the compiler. The second type is the failure in finding a valid site mapping. This happens when the machine contains many sites (>100), and the compilation will time out. This problem has high complexity, so optimization by the device may be desired. The last type is induced by the solver failing to generate a solution to the mixed-binary equation (solver time out).

We first study the effect of topology and machine sizes on the compilation time of the MIS Hamiltonians via SimuQ. We set the discretization number to 1. Here we use three kinds of topologies E : chains, cycles, and grids. The compilation times are presented in Table 5. For a typical IBM machine topology, it is easy to find a site mapping for a chain, hard for a cycle, and impossible for a grid. Furthermore, these compilations require a large number of equations. To synthesize a 40-vertex chain on a 127-qubit IBM machine, 862 equations are built upon 1771 variables, which on average takes around 2 minutes to solve. Similarly, while compilation to small Rydberg systems

Topology Backend	Chain (N)				Cycle (N)				Grid ($N \times N$)	
	6	12	20	40	6	12	20	40	3x3	4x4
Bloqade	0.257	1.28	4.03	83.8	0.471	14.6	573	>1000	143	>1000
IBM Pulse	3.43	5.34	10.5	151	N.A.	5.66	13.3	>1000	N.A.	N.A.
IonQ Circuit	0.678	4.43	43.7	N.A.	0.676	6.74	33.8	N.A.	2.64	15.46

Table 5. Compilation time (unit: s) of MIS Hamiltonians on backend machines. The discretization number and Trotterization number are set to 1. N.A. represents cases where SimuQ compiler returns no solution. >1000 represents a timed-out compilation. A chain contains $N - 1$ edges connecting vertex i and vertex $i + 1$. A cycle, compared to the chain graphs, additionally contains an edge connecting vertex N and vertex 1. A grid graph contains vertices labeled by integer pairs (i, j) , and connects (i, j) to $(i + 1, j)$ and $(i, j + 1)$.

Evolution Backend	MIS (D)				QAOA (D)				Heis (D)
	1	5	10	20	1	5	10	20	1
Bloqade	2.00	24.0	80.2	334	N.A.	N.A.	N.A.	N.A.	N.A.
IBM Pulse	8.7	32.7	70	156	4.13	21.4	37.9	115	1.34
IonQ Circuit	13.7	57.4	111	167	7.67	36.8	98.1	216	1.19

Table 6. Compilation time (unit: s) of different evolution and discretization numbers on different backend machines. Here Trotterization number is set to 1, and D is the discretization number. N.A. represents cases where SimuQ compiler returns no solution. >1000 represents a timed-out compilation. The MIS Hamiltonian is on a 15-qubit chain. The QAOA problems are instantiated on a 12-vertex graph, where D represents the layer number p in the setting. The Heisenberg model instantiated on a 7-site topology of IBM’s machines is a time-independent model, so we only consider $D = 1$ for it.

is fast, solving for atom positions in large Rydberg systems is hard without heuristics because of the highly non-linear interaction strength and the large search space. In contrast, IonQ machines have full connectivity, so site mapping is trivial and the compilation is fast. However, because their machines have at most 21 qubits, compilation for problems with more than 21 sites fails.

Second, we test the effect of the discretization number and different Hamiltonians on the compilation time and present our results in Table 6. We apply SimuQ to compile the MIS Hamiltonian, Max-Cut QAOA evolution, and Heisenberg model to the machines using different discretization numbers D . The compilation times for IBM machines and IonQ machines are almost linear in the discretization number because they do not have global variables, so each piece of constant Hamiltonian evolution can be dealt with independently. For Rydberg systems, the time complexity has a higher-order dependency on the discretization number because the presence of global variables requires all pieces to be solved together. The compilations for QAOA evolution and the Heisenberg model fail for Rydberg systems because of a lack of engineered pulses realizing single-site evolution.

6 CONCLUSION AND FUTURE DIRECTIONS

The domain-specific language SimuQ described in this paper is the first framework to consider quantum simulation and compilation to multiple platforms of analog quantum devices. We propose HML for front-end users to intuitively program their target quantum systems. We also design abstract analog instruction sets to depict the programmability of analog quantum devices and the AAIS Specification Language to program them. Besides, the SimuQ compiler is the first compiler of its kind to generate pulse schedules of analog quantum devices for desired quantum simulation problems.

Since this is the first feasibility demonstration of programming analog quantum devices, there is much optimization space for our compiler. First of all, since different devices have different

properties crucial to the compiler’s efficiency, we may develop compilation passes specifically for each platform. Second, in this paper, we employ a brute-force search with heuristics to find a site mapping, where more pruning techniques are desired. The hand-crafted mixed-binary equation solver can also be optimized according to the structure of the problem. At last, we may add more compilation techniques like [Clinton et al. 2021] to synthesize product Haimltonians not appearing directly in the given AAIS with a combination of instruction calls.

ACKNOWLEDGMENTS

Y.P., J.Y., and X.W. were partially funded by the U.S. Department of Energy, Office of Science, Office of Advanced Scientific Computing Research, Quantum Testbed Pathfinder Program under Award Number DE-SC0019040, Air Force Office of Scientific Research under award number FA9550-21-1-0209, and the U.S. National Science Foundation grant CCF-1942837 (CAREER).

REFERENCES

Ali J Abhari, Arvin Faruque, Mohammad J Dousti, Lukas Svec, Oana Catu, Amlan Chakrabati, Chen-Fu Chiang, Seth Vanderwilt, John Black, and Fred Chong. 2012. *Scaffold: Quantum programming language*. Technical Report. Princeton Univ NJ Dept of Computer Science.

Sara Achour and Martin Rinard. 2020. Noise-Aware Dynamical System Compilation for Analog Devices with Legno. In *Proceedings of the Twenty-Fifth International Conference on Architectural Support for Programming Languages and Operating Systems (ASPLOS ’20)*. Association for Computing Machinery, New York, NY, USA, 149–166. <https://doi.org/10.1145/3373376.3378449>

Sara Achour, Rahul Sarpeshkar, and Martin C. Rinard. 2016. Configuration Synthesis for Programmable Analog Devices with Arco. In *Proceedings of the 37th ACM SIGPLAN Conference on Programming Language Design and Implementation (PLDI ’16)*. Association for Computing Machinery, New York, NY, USA, 177–193. <https://doi.org/10.1145/2908080.2908116>

Thomas Alexander, Naoki Kanazawa, Daniel J Egger, Lauren Capelluto, Christopher J Wood, Ali Javadi-Abhari, and David C McKay. 2020. Qiskit pulse: Programming quantum computers through the cloud with pulses. *Quantum Science and Technology* 5, 4 (2020), 044006.

John Backus. 1978. *The History of Fortran I, II, and III*. Association for Computing Machinery, New York, NY, USA, 25–74. <https://doi.org/10.1145/800025.1198345>

Lucas Beguin, Aline Vernier, Radu Chicireanu, Thierry Lahaye, and Antoine Browaeys. 2013. Direct measurement of the van der Waals interaction between two Rydberg atoms. *Physical review letters* 110, 26 (2013), 263201.

Colin D Bruzewicz, John Chiaverini, Robert McConnell, and Jeremy M Sage. 2019. Trapped-ion quantum computing: Progress and challenges. *Applied Physics Reviews* 6, 2 (2019), 021314.

Andrew M. Childs, Dmitri Maslov, Yunseong Nam, Neil J. Ross, and Yuan Su. 2018. Toward the first quantum simulation with quantum speedup. *Proceedings of the National Academy of Sciences* 115, 38 (2018), 9456–9461.

Laura Clinton, Johannes Bausch, and Toby Cubitt. 2021. Hamiltonian simulation algorithms for near-term quantum hardware. *Nature communications* 12, 1 (2021), 4989.

Iris Cong, Harry Levine, Alexander Keesling, Dolev Bluvstein, Sheng-Tao Wang, and Mikhail D Lukin. 2022. Hardware-efficient, fault-tolerant quantum computation with Rydberg atoms. *Physical Review X* 12, 2 (2022), 021049.

Andrew Cross, Ali Javadi-Abhari, Thomas Alexander, Niel De Beaudrap, Lev S. Bishop, Steven Heidel, Colm A. Ryan, Prasahnt Sivarajah, John Smolin, Jay M. Gambetta, and Blake R. Johnson. 2022. OpenQASM 3: A Broader and Deeper Quantum Assembly Language. *ACM Transactions on Quantum Computing* 3, 3, Article 12 (sep 2022), 50 pages. <https://doi.org/10.1145/3505636>

Shantanu Debnath, Norbert M Linke, Caroline Figgatt, Kevin A Landsman, Kevin Wright, and Christopher Monroe. 2016. Demonstration of a small programmable quantum computer with atomic qubits. *Nature* 536, 7614 (2016), 63–66.

Sepehr Ebadi, Alexander Keesling, Madelyn Cain, Tout T Wang, Harry Levine, Dolev Bluvstein, Giulia Semeghini, Ahmed Omran, J-G Liu, Rhine Samajdar, et al. 2022. Quantum optimization of maximum independent set using Rydberg atom arrays. *Science* (2022), eab06587.

Sepehr Ebadi, Tout T. Wang, Harry Levine, Alexander Keesling, Giulia Semeghini, Ahmed Omran, Dolev Bluvstein, Rhine Samajdar, Hannes Pichler, Wen Wei Ho, Soonwon Choi, Subir Sachdev, Markus Greiner, Vladan Vuletić, and Mikhail D. Lukin. 2021. Quantum phases of matter on a 256-atom programmable quantum simulator. *Nature* 595, 7866 (2021), 227–232.

Alexander S. Green, Peter LeFanu Lumsdaine, Neil J. Ross, Peter Selinger, and Benoît Valiron. 2013. Quipper: A Scalable Quantum Programming Language. In *Proceedings of the 34th ACM SIGPLAN Conference on Programming Language*

Design and Implementation (PLDI '13). Association for Computing Machinery, New York, NY, USA, 333–342. <https://doi.org/10.1145/2491956.2462177>

Nikodem Grzesiak, Reinholt Blümel, Kenneth Wright, Kristin M Beck, Neal C Pisenti, Ming Li, Vandiver Chaplin, Jason M Amini, Shantanu Debnath, Jwo-Sy Chen, et al. 2020. Efficient arbitrary simultaneously entangling gates on a trapped-ion quantum computer. *Nature communications* 11, 1 (2020), 1–6.

David Hayes, Steven T Flammia, and Michael J Biercuk. 2014. Programmable quantum simulation by dynamic Hamiltonian engineering. *New Journal of Physics* 16, 8 (2014), 083027.

Kesha Hietala, Robert Rand, Shih-Han Hung, Xiaodi Wu, and Michael Hicks. 2021. A Verified Optimizer for Quantum Circuits. *Proc. ACM Program. Lang.* 5, POPL, Article 37 (jan 2021), 29 pages. <https://doi.org/10.1145/3434318>

J.R. Johansson, P.D. Nation, and Franco Nori. 2012. QuTiP: An open-source Python framework for the dynamics of open quantum systems. *Computer Physics Communications* 183, 8 (2012), 1760–1772. <https://doi.org/10.1016/j.cpc.2012.02.021>

Petar Jurcevic, Ali Javadi-Abhari, Lev S Bishop, Isaac Lauer, Daniela F Bogorin, Markus Brink, Lauren Capelluto, Oktay Günlük, Toshinari Itoko, Naoki Kanazawa, et al. 2021. Demonstration of quantum volume 64 on a superconducting quantum computing system. *Quantum Science and Technology* 6, 2 (2021), 025020.

A Yu Kitaev. 1997. Quantum computations: algorithms and error correction. *Russian Mathematical Surveys* 52, 6 (1997), 1191.

Junyi Liu, Bohua Zhan, Shulng Wang, Shenggang Ying, Tao Liu, Yangjia Li, Mingsheng Ying, and Naijun Zhan. 2019. Formal verification of quantum algorithms using quantum hoare logic. In *International conference on computer aided verification*. Springer, 187–207.

Kristen Nygaard and Ole-Johan Dahl. 1978. *The Development of the SIMULA Languages*. Association for Computing Machinery, New York, NY, USA, 439–480. <https://doi.org/10.1145/800025.1198392>

John Preskill. 2018. Quantum computing in the NISQ era and beyond. *Quantum* 2 (2018), 79.

QuEra. 2022. Bloqade: a Julia package for quantum computation and quantum dynamics based on neutral-atom architectures. <https://queracomputing.github.io/Bloqade.jl/dev/>

Mark Saffman. 2016. Quantum computing with atomic qubits and Rydberg interactions: progress and challenges. *Journal of Physics B: Atomic, Molecular and Optical Physics* 49, 20 (2016), 202001.

G. Semeghini, H. Levine, A. Keesling, S. Ebadi, T. T. Wang, D. Bluvstein, R. Verresen, H. Pichler, M. Kalinowski, R. Samajdar, A. Omran, S. Sachdev, A. Vishwanath, M. Greiner, V. Vuletić, and M. D. Lukin. 2021. Probing topological spin liquids on a programmable quantum simulator. *Science* 374, 6572 (2021), 1242–1247.

Yunong Shi, Pranav Gokhale, Prakash Murali, Jonathan M. Baker, Casey Duckering, Yongshan Ding, Natalie C. Brown, Christopher Chamberland, Ali Javadi-Abhari, Andrew W. Cross, David I. Schuster, Kenneth R. Brown, Margaret Martonosi, and Frederic T. Chong. 2020. Resource-Efficient Quantum Computing by Breaking Abstractions. *Proc. IEEE* 108, 8 (2020), 1353–1370. <https://doi.org/10.1109/JPROC.2020.2994765>

Henrique Silvério, Sebastián Grijalva, Constantin Dalyac, Lucas Leclerc, Peter J. Karalekas, Nathan Shammah, Mourad Beji, Louis-Paul Henry, and Loïc Henriet. 2022. Pulser: An open-source package for the design of pulse sequences in programmable neutral-atom arrays. *Quantum* 6 (Jan. 2022), 629. <https://doi.org/10.22331/q-2022-01-24-629>

Matthias Steffen, David P DiVincenzo, Jerry M Chow, Thomas N Theis, and Mark B Ketchen. 2011. Quantum computing: An IBM perspective. *IBM Journal of Research and Development* 55, 5 (2011), 13–1.

A DETAILS OF EQ2.2.1

$$\begin{aligned}
 \frac{C}{4(x_1 - x_2)^6} &= 1 & (Z_1 Z_2) \\
 \frac{C}{4(x_2 - x_3)^6} &= 1 & (Z_2 Z_3) \\
 \frac{C}{4(x_1 - x_3)^6} &= 0 & (Z_1 Z_3) \\
 -\frac{C}{4(x_1 - x_2)^6} - \frac{C}{4(x_1 - x_3)^6} + \frac{\Delta_{t_1}}{2} \cdot s_{t_1} &= -\frac{1}{2} & (Z_1) \\
 -\frac{C}{4(x_1 - x_2)^6} - \frac{C}{4(x_2 - x_3)^6} + \frac{\Delta_{t_2}}{2} \cdot s_{t_2} &= -\frac{3}{2} & (Z_2) \\
 -\frac{C}{4(x_1 - x_3)^6} - \frac{C}{4(x_2 - x_3)^6} + \frac{\Delta_{t_3}}{2} \cdot s_{t_3} &= -\frac{1}{2} & (Z_3) \\
 \frac{\Omega_{t_1} \cos(\phi_{t_1})}{2} \cdot s_{t_1} &= 2 & (X_1) \\
 \frac{\Omega_{t_2} \cos(\phi_{t_2})}{2} \cdot s_{t_2} &= 2 & (X_2) \\
 \frac{\Omega_{t_3} \cos(\phi_{t_3})}{2} \cdot s_{t_3} &= 2 & (X_3) \\
 \frac{\Omega_{t_1} \sin(\phi_{t_1})}{2} \cdot s_{t_1} &= 0 & (Y_1) \\
 \frac{\Omega_{t_2} \sin(\phi_{t_2})}{2} \cdot s_{t_2} &= 0 & (Y_2) \\
 \frac{\Omega_{t_3} \sin(\phi_{t_3})}{2} \cdot s_{t_3} &= 0 & (Y_3)
 \end{aligned}$$

B DETAILS OF AAISS FOR QUERA, IBM, IONQ'S MACHINES

QuEra's Rydberg atom arrays. QuEra's Rydberg systems put neutral atoms in a 2-D space and apply configurable lasers to influence these atoms. These machines are very similar to the ideal Rydberg machine discussed in Section 2.2.1 but only allow global laser control. That is, all atoms are affected by the same laser beam. For an N -qubit system, the Hamiltonian is

$$H(t) = -\Delta(t) \sum_{i=1}^N \hat{n}_i + \frac{\Omega(t)}{2} \sum_{i=1}^N X_i + \sum_{i < j} \frac{C}{d^6(i, j)} \hat{n}_i \hat{n}_j.$$

Here $C = 5.42 \times 10^6$. We design the AAIS for these machines like the ideal Rydberg machine. The positions of atoms are modeled as an array of global variables, and the system Hamiltonian is $\sum_{i < j} \frac{C}{d^6(i, j)} \hat{n}_i \hat{n}_j$ where $d(i, j)$ calculates the distance between atoms i and j from the global variables. We design a signal line for the laser beam. An instruction is constructed with three variables modeling detuning Δ , amplitude Ω , and phase ϕ . The instruction Hamiltonian is then $\sum_{i=1}^N (-\Delta \hat{n}_i + \Omega(\cos(\phi_i) X_i - \sin(\phi_i) Y_i))$.

IBM's superconducting systems. IBM's superconducting quantum processors are constructed from superconducting artificial atoms—fixed-frequency anharmonic oscillators, each with dedicated drive and readout lines and coupled to neighboring qubits. The Hamiltonian of an n -qubit IBM

machine is

$$H(t) = \sum_{j=1}^n \sum_{k \in E_j} \Omega_j \mathcal{M}_{jk}(u_{jk}, t) X_j + \sum_{j=1}^n \epsilon_j n_j + \sum_{\substack{(j,k) \in E \\ j \neq k}} \frac{J_{jk}}{4} (X_j X_k + Y_j Y_k), \quad (\text{B.0.1})$$

where E is a bidirectional connectivity graph with self loops, $J_{jk} = J_{kj}$, and Ω_j is the maximal energy input on qubit j . Function $u_{jk}(t)$ is a complex valued function representing the control microwave pulse. Modulation $\mathcal{M}_{jk}(u_{jk}, t)$ modulates pulse u_{jk} with a local oscillatory frequency ω_k of qubit k : $\mathcal{M}_{jk}(u_{jk}, t) = \text{Re}\{e^{i\omega_k t} u_{jk}(t)\}$. We view interactions with each quantum system on the device in a reference frame oscillating at its resonant frequency, and in this perspective, qubit j has a drive Hamiltonian given by

$$H_j(t) = \Omega_j(t) (\cos(\phi_j(t)) X_j + \sin(\phi_j(t)) Y_j). \quad (\text{B.0.2})$$

One can also realize free Z gates by adding phases to all future gates applied on a qubit. Entangling operations are performed on coupled qubits by driving one qubit at another's frequency, and in the rotating frame, this interaction is effectively Hamiltonian $v_{ZX} Z_i X_j + v_{IX} X_j + v_{IZ} Z_j + v_{ZI} Z_i + v_{ZZ} Z_i Z_j$, where v 's are a set of coefficients. By applying an echoing drive, we can cancel out most side effects, and the remaining effect is $Z_i X_j$. Combined with basis changes via one-qubit gates, these pulses realized evolution under $X_i X_j$, $Y_i Y_j$ and $Z_i Z_j$.

Notice the permanent system Hamiltonian $\sum_{(j,k) \in E, j \neq k} \frac{J_{jk}}{4} (X_j X_k + Y_j Y_k)$ exists. However, its influence on the state is a small oscillation that can be neglected when idling. Hence we build the AAIS without a system Hamiltonian.